A Quantitative Model of Purinergic Junctional Transmission of Calcium Waves in Astrocyte Networks

M. R. Bennett,* L. Farnell,† and W. G. Gibson†
*The Neurobiology Laboratory, Institute for Biomedical Research, Department of Physiology, and †The School of Mathematics and Statistics, University of Sydney, New South Wales, Australia

ABSTRACT A principal means of transmitting intracellular calcium (Ca^{2+}) waves at junctions between astrocytes involves the release of the chemical transmitter adenosine triphosphate (ATP). A model of this process is presented in which activation of purinergic P2Y receptors by ATP triggers the release of ATP, in an autocrine manner, as well as concomitantly increasing intracellular Ca^{2+}. The dependence of the temporal characteristics of the Ca^{2+} wave are shown to critically depend on the dissociation constant (K_R) for ATP binding to the P2Y receptor type. Incorporating this model astrocyte into networks of these cells successfully accounts for many of the properties of propagating Ca^{2+} waves, such as the dependence of velocity on the type of P2Y receptor and the time-lag of the Ca^{2+} wave behind the ATP wave. In addition, the conditions under which Ca^{2+} waves may jump from one set of astrocytes across an astrocyte-free lane to another set of astrocytes are quantitatively accounted for by the model. The properties of purinergic transmission at astrocyte junctions may determine many of the characteristics of Ca^{2+} propagation in networks of these cells.

INTRODUCTION

Purinergic receptors on astrocytes implicated in Ca^{2+} elevation

Application of adenosine triphosphate (ATP) to astrocytes for periods of several hundred seconds gives rise to a transient increase in Ca^{2+} concentration—hereafter denoted by $[Ca^{2+}]$—which then relaxes to a maintained plateau (1–3, but see Koizumi et al. (4)). The sustained response is due to an influx of calcium ions through $P2X_7$ receptors (1,5). The transient response is most likely mediated by $P2Y_1$ and $P2Y_2$ receptors (henceforth $P2Y_1$ R and $P2Y_2$ R), involving an increase in inositol 1,4,5-trisphosphate (IP_3) to release calcium from endoplasmic reticulum (ER) stores (4) through G-protein coupling to phospholipase C (PLC) (3,6). The $P2Y_2$ R agonist uridine 5′-triphosphate (UTP) produces Ca^{2+} in astrocytes through an increase in IP_3 turnover (7) with subsequent release of calcium from thapsigargin-sensitive calcium stores (8) as well as release of ATP (9); however, the mechanism by which ATP is released is as yet unknown. Direct evidence for the existence of functional $P2Y_1$ R and $P2Y_2$ R on astrocytes has been obtained by injecting astrocyte mRNA into oocytes and showing subsequently that these give Ca^{2+} upon application of the $P2Y_1$ R agonist 2-methylthio ATP and the $P2Y_2$ R agonist UTP (10); see also Zhu and Kimelberg (11). The dominant metabotropic P2YR appears to be $P2Y_1$ R, according to a combined Western blot pharmacological approach (12).

Involvement of P2Y receptors in junctional transmission of Ca^{2+} between astrocytes

Hassinger et al. (13) have shown that scraping away cells to form a cell-free lane in two-dimensional astrocyte cultures does not interrupt the Ca^{2+} initiated on one side of the lane from propagating to the other side for lane widths $<\sim 120$ μm, although the delay time for the Ca^{2+} propagating across the lane is longer the wider the lane. These observations show that transmission of Ca^{2+} may involve the release of a chemical substance from the astrocytes. It is very likely that the principal substance that mediates this Ca^{2+} transmission is ATP. Simultaneous imaging of ATP and Ca^{2+} waves in two-dimensional cortical astrocyte cultures have been obtained after these were initiated by mechanical stimulation of an astrocyte (14). Both waves possess a duration of $\sim$10s at half-height and both were blocked by the purinergic receptor antagonist suramin. P2YRs, specifically $P2Y_1$ Rs and $P2Y_2$ Rs, dominate in the action of the astrocyte transmitter ATP in propagating Ca^{2+} waves (see, for example, Gallagher and Salter (15) and Salter and Hicks (16)). In spinal cord astrocytes, specific $P2Y_1$ R antagonists, such as adenosine-3′-phospho-5′-phosphosulfate, block transmission (17); see also Fam et al. (18). A fivefold greater concentration of the $P2Y_2$ R agonist UTP is required to give a $[Ca^{2+}]$ comparable to that obtained using the specific $P2Y_1$ R agonist 2-MeS adenosine diphosphate (henceforth, ADP) (18), although ATP itself is equipotent at $P2Y_1$ Rs and $P2Y_2$ Rs (19). Gallagher and Salter (15) have shown that transmission of Ca^{2+} occurs in two-dimensional cultures of human astrocytoma cells heterologously expressing either $P2Y_1$ Rs or $P2Y_2$ Rs, with transmission through the latter faster than through the former. They take this to be due to the fact that $P2Y_1$ Rs take longer than $P2Y_2$ Rs to generate Ca^{2+} when stimulated

Submitted March 14, 2005, and accepted for publication June 30, 2005.

Address reprint requests to Professor Max Bennett, Neurobiology Laboratory, Dept. of Physiology, University of Sydney, NSW 2006, Australia. Tel.: 61-2-9351-2034; Fax: 61-2-9351-3910; E-mail: maxb@physiol.usyd.edu.au.

0006-3495/05/10/2235/16 $2.00

doi: 10.1529/biophysj.105.062968

with ATP. Since ADP acting on $P2Y_1$ Rs generates Ca^{2+} much faster than ATP, therefore apyrase, by metabolizing ATP to ADP, accelerates Ca^{2+} release in astrocytes that only express $P2Y_1$ Rs but blocks release in astrocytes that only express $P2Y_2$ Rs (15). Although glutamate receptors exist on astrocytes, the release of glutamate onto these is not primarily involved in the transmission of Ca^{2+} waves, but rather that of Na^+ waves (20).

Mechanism of release of ATP from astrocytes during junctional transmission of Ca^{2+}

It is well established that ATP-stimulated release of glutamate from astrocytes involves a calcium-triggered exocytosis of glutamate-containing vesicles (21–24). However, the mechanism of release of ATP from astrocytes has yet to be clearly established. Mechanical stimulation gives rise to an increase in $[Ca^{2+}]$, which, if buffered with BAPTA, has been claimed either to block (25,26) or not to block (14) ATP release. However, depletion of intracellular calcium stores with thapsigargin fails to block ATP release (14). Most importantly, ATP waves propagate ahead of calcium waves from the point of stimulation in a two-dimensional astrocyte culture (14) and in the retina (27). Thus, the cumulative evidence is against a Ca^{2+}-dependent exocytosis of ATP. Alternative pathways for ATP release from astrocytes that are not dependent on calcium-triggered exocytosis are possible. ATP release is partially blocked by antagonists to ATP-binding-cassette proteins such as glibenclamide (28,9) and there is evidence that elevation of protein kinase C (PKC) enhances a glibenclamide-sensitive chloride efflux from astrocytes through ATP-binding cassette proteins, raising the possibility that PKC stimulation elevates ATP release (28).

Modeling the process of astrocyte junctional transmission of Ca^{2+}

Previous models of Ca^{2+} wave propagation in networks of glial cells have assumed that the passive diffusion of IP_3 through gap junctions is the underlying mechanism (29,30). An elevated concentration of IP_3 in a single cell acts on receptors on the ER causing the release of Ca^{2+} into the cytosol, which then activates PLC to produce more IP_3. This IP_3 diffuses to neighboring cells, where the regenerative process is repeated. In contrast, the present model is based solely on purinergic transmission, where the underlying mechanism is the diffusion of ATP in the extracellular space. This ATP binds to P2Y receptors on the astrocyte surface, thus initiating a G-protein cascade that leads to the production of IP_3 and the consequent release of Ca^{2+} from internal stores. This increase in $[IP_3]$ is also assumed to lead to release of ATP into the extracellular space, where it acts back on the initiating cell and also diffuses to neighboring cells, thus propagating an ATP wave and a Ca^{2+} wave. We consider both one-dimensional and two-dimensional networks of these astrocytes and show that the model accounts for most observations on astrocytic transmission and provides a coherent theoretical framework for further experimental research on this subject.

METHODS

Overview

The single-cell model follows that of Lemon et al. (31) with some changes. Simplifications have been made: some processes included in that model are not relevant to astrocytes; others are second-order effects and can be omitted with little change to the final results. The main additions that must be made concern the release of ATP into the extracellular space and the diffusion of IP_3 inside the cell and ATP outside the cell. Fig. 1 *A* is a schematic diagram showing the main processes that will be used in our model of a single cell; Table 1 gives the parameter values used in the calculations.

Receptors

A basic model is used in which receptors do not desensitize—they are neither phosphorylated nor internalized and recycled. Thus the reaction is

$$L + R \underset{k_l^-}{\overset{k_l^+}{\rightleftarrows}} LR, \tag{1}$$

where L is ligand and R receptor. The quantity we want is the ratio of bound to total receptors, $\rho = [LR]/[R_T]$, where $[R_T] = [R] + [LR]$ is the total number of receptors. Under the assumption of fast binding kinetics, Eq. 1 can be assumed to be in equilibrium, leading to

$$\rho = \frac{[ATP]}{K_R + [ATP]}, \tag{2}$$

where $[L] = [ATP]$ is the extracellular ATP concentration and $K_R = k_l^-/k_l^+$ is the dissociation constant. Although K_R is defined in relation to the binding of ATP to P2Y receptors, and as such should have a value of the order of 10 μM (32), it can be interpreted more broadly in the context of the model. The crucial quantity is ρ, since this governs the production of active G-protein (see Eq. 3 below), and thus ρ can be interpreted more generally as being a measure of additional aspects of the model such as the density of P2Y receptors and the strength of the coupling of the bound receptors to G-protein activation. To save introducing additional parameters, these aspects have been incorporated in the single quantity K_R, which then becomes an effective, rather than an actual, dissociation constant.

G-protein cascade

The equation describing G-protein activation is Lemon et al. (31), their Eq. 16:

$$\frac{d[G]}{dt} = k_a(\delta + \rho)([G_T] - [G]) - k_d[G], \tag{3}$$

where $[G]$ is the amount of activated G-protein, $[G_T]$ is the total G-protein, ρ is the fraction of bound receptors as given by Eq. 2, δ is the ratio of the activities of the unbound and bound receptors (and thus allows for background activity even in the absence of ligand binding, i.e., unbound receptors can activate a small amount of G-protein), and k_a and k_d are the G-protein activation and deactivation rate parameters, respectively. Eq. 3 is represented by the kinetic scheme

$$G_{in} \underset{k_d}{\overset{k_a(\rho+\delta)}{\rightleftarrows}} G, \tag{4}$$

TABLE 1 Model parameter values

Symbol	Definition	Value	Notes
P2Y Receptor regulation			
K_R	Dissociation constant for ligand binding to P2YRs	Various	See text
G-protein cascade			
k_{deg}	IP_3 degradation rate	1.25 s^{-1}	(31)
k_a	G-protein activation rate	0.017 s^{-1}	(31)
k_d	G-protein deactivation rate	0.15 s^{-1}	(31)
r_h^*	IP_3 production rate	2×10^{-14} μmol μm^{-2} s^{-1}	Fit to experiment
D_{IP}	IP_3 diffusion coefficient	280 μm^2 s^{-1}	(30)
ATP production			
V_{ATP}	ATP production rate	2×10^{-11} μmol μm^{-2} s^{-1}	Fit to experiment
K_{rel}	Kinetic parameter	10 μM	Fit to experiment
$[IP_3]_{min}$	Threshold concentration	0.012 μM	Fit to experiment
k_{loss}	Depletion rate parameter	30 s^{-1}	Fit to experiment
D_{ATP}	ATP diffusion coefficient	300 μm^2 s^{-1}	(67)
J_{max}	Maximum channel current	2880 μM s^{-1}	(36)
K_I	IP_3 channel kinetic parameter	0.03 μM	(36)
K_{act}	IP_3 channel kinetic parameter	0.17 μM	(36)
k_{on}	IP_3 channel kinetic parameter	8.0 μM s^{-1}	(36)
K_{inh}	IP_3 channel kinetic parameter	0.1 μM	(36)
$[Ca^{2+}_{ER}]$	Ca^{2+} concentration in ER	400 μM	(36)
V_{max}	Maximum pumping rate into ER	5.85 μM s^{-1}	(36)
K_p	Pump dissociation constant	0.24 μM	(36)
β	Endogenous buffer parameter	0.0244	(36)
Initial values			
$[IP_3]_0$	Initial IP_3 concentration	0.01 μM	(31)
$[Ca^{2+}]_0$	Initial Ca^{2+} concentration	0.05 μM	(36)

where G_{in} is inactive G-protein, so $[G_{in}] = [G_T] - [G]$. Again assuming fast kinetics, we obtain

$$G^* = \frac{\rho + \delta}{K_G + \delta + \rho}, \tag{5}$$

where $G^* = [G]/[G_T]$ and $K_G = k_d/k_a$.

IP_3 production and diffusion

IP_3 production and degradation is governed by Lemon et al. (31), their Eq. 19:

$$\frac{d[IP_3]}{dt} = r_h[PIP_2] - k_{deg}[IP_3], \tag{6}$$

where $r_h = \alpha([Ca^{2+}]/(K_c + [Ca^{2+}]))[G]$ and the last term accounts for the degradation of IP_3 inside the cell. The Ca^{2+}-dependence of r_h allows for the catalytic effect of Ca^{2+} on IP_3 production (it binds to a catalytic site on PLC), but for simplicity this secondary effect is not included in the astrocyte model, so $K_c = 0$ giving $r_h = \alpha[G]$. Also, there is assumed to be no depletion of PIP_2, so $[PIP_2] = [(PIP_2)_T]$ and Eq. 6 simplifies to

$$\frac{d[IP_3]}{dt} = r_h^* G^* - k_{deg}[IP_3], \tag{7}$$

where G^* is given by Eq. 5, and r_h^* is a constant, independent of $[Ca^{2+}]$.

In the above equations $[IP_3]$ is taken to be spatially homogeneous, but now diffusion must be included. IP_3 is produced at the cell wall, it then diffuses into the cytosol and is degraded everywhere, including at the cell wall. Thus $[IP_3]$ is now spatially inhomogeneous, $[IP_3] = [IP_3](\mathbf{r}, t)$, and satisfies

$$\frac{\partial[IP_3]}{\partial t} = D_{IP}\nabla^2[IP_3] + r_h^* G^* - k_{deg}[IP_3], \tag{8}$$

where D_{IP} is the diffusion coefficient for IP_3 and the term $r_h^* G^*$ is applied only at the cell wall.

ATP production and diffusion

As stated in the Introduction (see also Discussion), the mechanism by which ATP is released by astrocytes has not been established, although there is evidence that IP_3 is probably involved. We have chosen to use IP_3 as the agent triggering release, but this is not crucial to the model. The release can be linked to the concentration of active G-protein, with essentially the same results. In an even simpler model, ATP release can be taken to depend directly on ATP concentration, with no intermediate steps.

ATP is assumed to be released into the extracellular space at the cell boundary at rate

$$V_{ATP}\chi(t)\frac{[IP_3] - [IP_3]_{min}}{K_{rel} + [IP_3]}, \tag{9}$$

provided $[IP_3]$ is greater than $[IP_3]_{min}$; otherwise it is not released. The threshold value $[IP_3]_{min}$ is necessary to prevent very small levels of [ATP] from being amplified and thus leading to a propagating wave. V_{ATP} and K_{rel} are constants and $\chi(t)$ is a parameter that accounts for depletion of ATP stores inside the cell; it has initial value 1 and decreases according to

$$\frac{d\chi}{dt} = -k_{loss}\chi(t)\frac{[IP_3] - [IP_3]_{min}}{K_{rel} + [IP_3]}, \tag{10}$$

where k_{loss} is a constant. This depletion is included to terminate ATP release from each cell and thus lead to the correct waveforms for [ATP] and $[Ca^{2+}]$. Some evidence for a depletable ATP store is provided by the observation that there is no ATP release by the third impulse during repetitive stimulation of astrocytes (14). Evidence against such depletion could come from experiments in which astrocytes are exposed to glutamate, leading to the

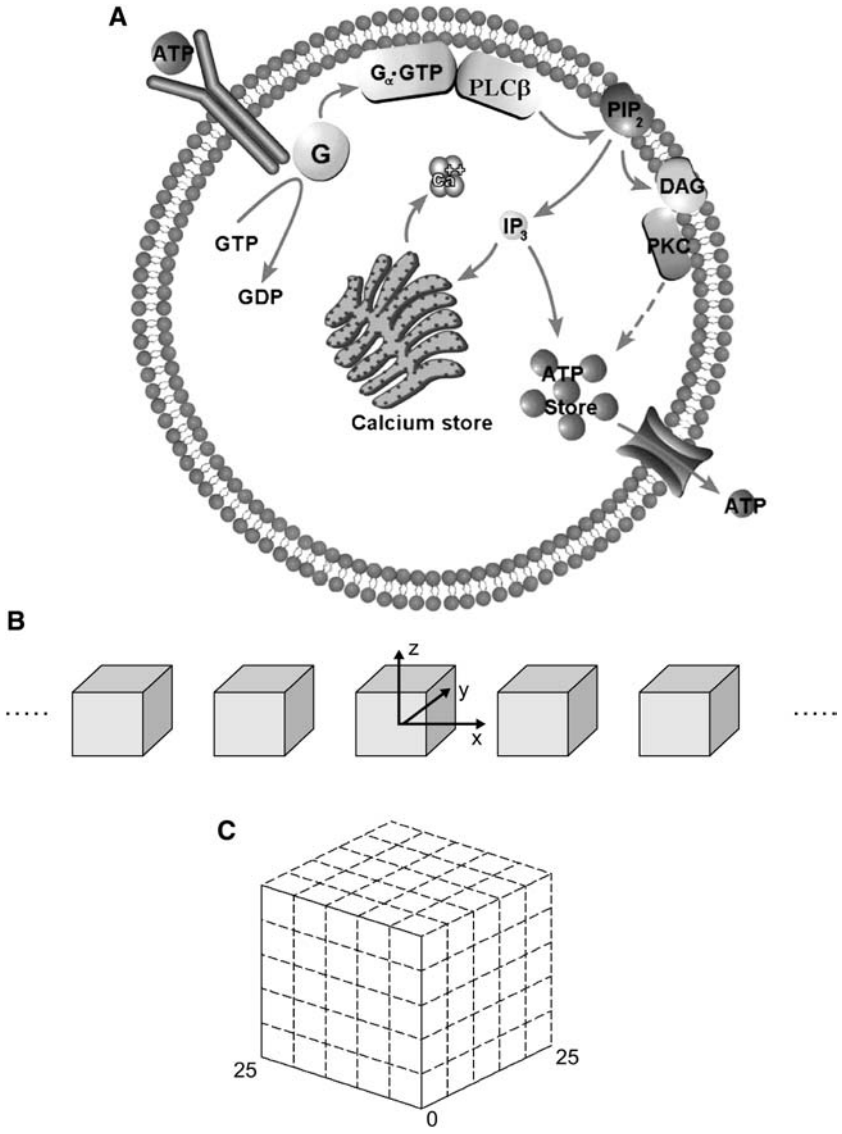

FIGURE 1 (*A*) Simplified schematic diagram of the steps leading from metabotropic receptor activation to Ca^{2+} release from the calcium store (endoplasmic reticulum) into the cytosol and ATP release from internal stores into the extracellular space. Transmitter (*ATP*) binds to the receptor which then interacts with the G-protein (*G*), leading to the replacement of GDP with GTP and the subsequent dissociation of the G-protein into subunits. The subunit G_α·GTP binds to a site on phospholipase C-β (*PLC*) and this activated unit initiates an interaction with membrane-bound phosphatidylinositol 4,5-bisphosphate (*PIP_2*), leading to the hydrolysis of PIP_2 and the production of IP_3. This diffuses into the cytosol where it opens IP_3-sensitive channels in the ER, allowing the release of Ca^{2+} into the cytosol. The IP_3 is also assumed to interact with ATP stores inside the astrocyte, leading to the release of ATP into the extracellular space. An alternative pathway, involving diacylglycerol (*DAG*) and protein kinase C (*PKC*) is also indicated, though it is not used in the present model. (*B*) A lane of model astrocytes, represented by cubes of side 25 μm, separated by spaces of width 25 μm. The cubes have their centers in the *xy* plane ($z = 0$) and are aligned parallel to the *x*-axis. (*C*) A cube of side 25 μm, representing a single astrocyte, subdivided into $5 \times 5 \times 5$ cubes of side 5 μm, as indicated by the broken lines. The grid points used in the numerical integration scheme are placed at the center of each subcube, thus giving 27 interior points and 98 surface points. At all points, the processes implemented are IP_3 diffusion and Ca^{2+} release from the ER; at the surface points, the additional processes implemented are receptor activation, the G-protein cascade leading to IP_3 production, and the release of ATP. The exterior space is likewise divided into subcubes of side 5 μm with grid points at the centers and these are used to implement diffusion of ATP in the extracellular space.

production of IP_3 and hence depletion of ATP stores, but an intercellular wave is still supported (33). However, it may be that only the initial response to glutamate releases significant quantities of IP_3: see especially Fig. 2 *A* in Kim et al. (34), which shows an initial Ca^{2+} spike followed by much lower oscillations. These oscillations might be supported by a concentration of IP_3 that is below threshold in our model, or they might be the result of Ca^{2+}-induced Ca^{2+} release from IP_3-insensitive stores (see Discussion in Charles et al. (33) and the theoretical analysis of Keizer and Levine (35)). Thus, the ATP stores may only be partially depleted by glutamate and also could have time for some refilling. An alternative way of terminating the action of ATP would be to assume that the P2Y receptors desensitize at a sufficient fast rate. Desensitization has been included in the P2Y receptor model in Lemon et al. (31), but the parameter values listed there give a timecourse that is too slow.

ATP diffuses in the extracellular space and is thus spatially inhomogeneous, [ATP] = [ATP](**r**, *t*), and satisfies

$$\frac{\partial[ATP]}{\partial t} = D_{\mathrm{ATP}}\nabla^2[ATP] + V_{\mathrm{ATP}}\chi\frac{[\mathrm{IP_3}] - [\mathrm{IP_3}]_{\mathrm{min}}}{K_{\mathrm{rel}} + [\mathrm{IP_3}]} - V_{\mathrm{deg}}\frac{[ATP]}{K_{\mathrm{deg}} + [ATP]}, \tag{11}$$

where D_{ATP} is the diffusion coefficient for ATP and the depletion term is applied only at the cell wall and only when $[\mathrm{IP_3}] > [\mathrm{IP_3}]_{\mathrm{min}}$. The last term allows for the breakdown of ATP by an ectonucleotidase. It was found that the inclusion of this term makes no essential difference to the output of the model (see Results) and so it has been omitted in the main calculations reported here.

Ca^{2+} release from internal stores

The steps leading from IP_3 production to Ca^{2+} release from the ER via IP_3 Rs have been modeled in Lemon et al. (31), but here we follow a similar scheme due to Fink et al. (36). Both schemes are based on the original models of De Young and Keizer (37), and Li and Rinzel (38).

The Ca^{2+} dynamics are governed by

$$\frac{d[\mathrm{Ca^{2+}}]}{dt} = \beta(J_{\mathrm{IP3}} - J_{\mathrm{pump}} + J_{\mathrm{leak}}), \tag{12}$$

where $[Ca^{2+}]$ is the cytosolic Ca^{2+} concentration, J_{IP3}, J_{pump}, and J_{leak} are the rates of Ca^{2+} concentration change due to release through IP_3 R channels, pump uptake into the ER, and leak from the ER, respectively, and

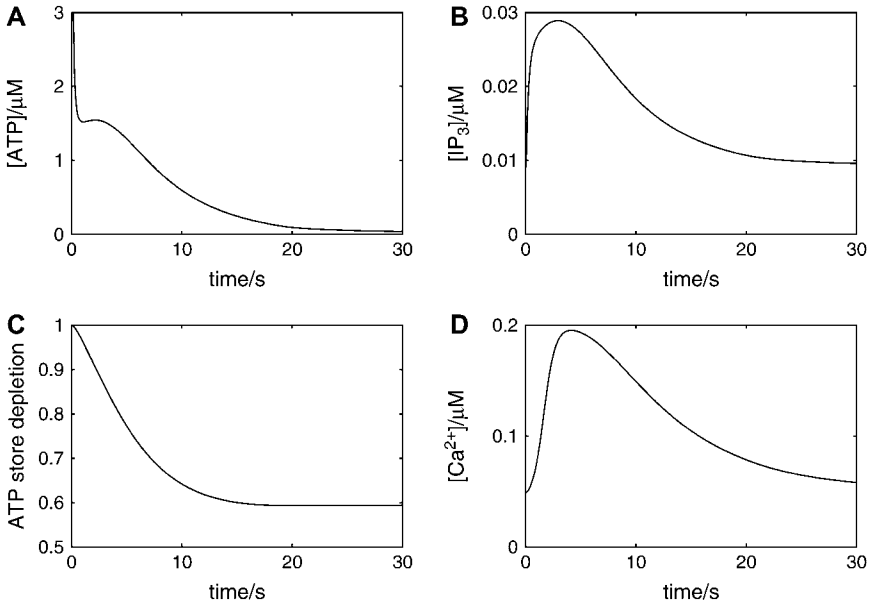

FIGURE 2 Changes in [ATP], $[IP_3]$, $[ATP]_{store}$, and $[Ca^{2+}]$ in a single isolated model astrocyte, as functions of time, after its exposure to an initiating instantaneous pulse of ATP of concentration 10 μM applied at time $t = 0$. (The pulse is applied at each grid point immediately surrounding the astrocyte.) $K_R = 25$ μM. (*A*) [ATP], immediately outside the astrocyte. (The initial amplitude is 10 μM, but the range on the ordinate has been reduced for clarity.) (*B*) $[IP_3]$, at the center of the astrocyte. (*C*) The depletion of the ATP store inside the astrocyte, expressed as a proportion of the initial [ATP]. (*D*) $[Ca^{2+}]$, at a point just inside the astrocyte.

β is a factor describing Ca^{2+} buffering. The diffusion of Ca^{2+} has been neglected, since it is much slower that that of IP_3. The IP_3-induced current is

$$J_{IP3} = J_{max}\left[\left(\frac{[IP_3]}{[IP_3]+K_I}\right)\left(\frac{[Ca^{2+}]}{[Ca^{2+}]+K_{act}}\right)h\right]^3\left[1-\frac{[Ca^{2+}]}{[Ca^{2+}]_{ER}}\right], \quad (13)$$

where J_{max} is the maximum rate, K_I is the dissociation constant for IP_3 binding to an IP_3 R, K_{act} is the dissociation constant for Ca^{2+} binding to an activation site on an IP_3 R, $[Ca^{2+}]_{ER}$ is the Ca^{2+} concentration in the ER (taken to be constant), and h satisfies

$$\frac{dh}{dt} = k_{on}[K_{inh} - ([Ca^{2+}]+K_{inh})h], \quad (14)$$

where k_{on} is the rate of Ca^{2+} binding to the inhibitory site on the IP_3 R and K_{inh} is the corresponding dissociation constant.

The ATPase Ca^{2+} pump is described by

$$J_{pump} = V_{max}\frac{[Ca^{2+}]^2}{[Ca^{2+}]^2+K_p^2}, \quad (15)$$

where V_{max} is the maximum pumping rate and K_p is the dissociation constant. The leak is described by

$$J_{leak} = P_L\left(1-\frac{[Ca^{2+}]}{[Ca^{2+}]_{ER}}\right), \quad (16)$$

where the constant P_L is determined by steady-state flux balance (see Initialization, below). The buffering is described by the steady-state approximation

$$\beta = \left(1+\frac{[B]_{end}}{K_{end}}\right)^{-1}, \quad (17)$$

where $[B]_{end}$ and K_{end} are the concentration and dissociation constants of the endogenous buffer, respectively.

Geometry

Each astrocyte is represented by a cube of side 25 μm (Fig. 1 *C*). These cubes are arranged in two-dimensional arrays, on the *x,y* plane. The minimum spacing between cubes is 25 μm, but this can be altered to investigate the maximum distance over which astrocytes can communicate. A single lane of four cubes with minimum spacing is illustrated in Fig. 1 *B*. In many calculations, lanes of 19 astrocytes were used in various configurations to investigate communication between lanes. With this simplified geometry we are not attempting to model the spatial complexity of a real astrocyte; rather this is an effective astrocyte in which the processes emanating from a real astrocyte are lumped into a compact space, taken to be cubical for reasons of computational simplicity. Real astrocytes also tend to be space-filling, with their arborizations touching but not overlapping (39); the intercellular gaps in our model reflect the fact that the specific geometry of the astrocytes has not been incorporated.

Initialization

In the absence of ATP there is still background IP_3 and Ca^{2+} resulting from the activation of a small amount of G-protein by unbound receptors (see Eq. 5; in this case, $\rho = 0$ but $\delta \neq 0$). If diffusion of IP_3 is neglected, then initial homogeneous concentrations of IP_3 and Ca^{2+}, $[IP_3]_0$, and $[Ca^{2+}]_0$ respectively, can be set. However, this cannot be used as the background state when diffusion is included, since the production of IP_3 at the cell wall and its subsequent diffusion into the interior of the cell violate this homogeneous state and lead to instabilities. Rather, these initial homogeneous concentrations are used to set the activity ratio δ (using Eqs. 5 and 7) as

$$\delta = \frac{K_G\, k_{deg}[IP_3]_0}{r_h^* - k_{deg}[IP_3]_0}, \quad (18)$$

and the Ca^{2+} leak rate, P_L, by setting $J_{IP3} - J_{pump} - J_{leak} = 0$. Then the IP_3 equation, Eq. 8, is run, as described in the following section, until a steady-state solution is obtained that is close to the homogeneous one, but of course not identical since it is inhomogeneous. The Ca^{2+} equation, Eq. 12, is now solved to find the corresponding equilibrium Ca^{2+} concentration, which will also be inhomogeneous (even though Ca^{2+} does not diffuse), because of the inhomogeneous distribution of IP_3.

Method of solution

Each cell is represented by a rectangular Cartesian grid with spacing 5 μm (Fig. 1 *C*), and thus contains 27 interior grid points and 98 surface grid points. The space between the cells is similarly represented by a rectangular

grid with the same spacing of 5 μm. The grid extends to ± 49 points in the z direction, which is essentially infinite. The lanes of 19 astrocytes use ± 99 grid points and thus the grid ends in a space between cells. The boundary conditions are ATP sinks at all boundaries. The ER is present at all 125 grid points of each cell and Ca^{2+} production and IP_3 degradation also occurs at each of these points. On the other hand, IP_3 production occurs only at the 98 surface points, as does ATP binding to P2YRs and the production of ATP.

The background distributions of IP_3 and Ca^{2+} are calculated as described in Initialization, above. In doing these calculations, fluxes need to be converted to concentration changes. A flux of f μmol μm^{-2} s^{-1} through an area a μm^2 into a volume v μm^3 leads to a concentration change of 10^{15} $(f\,a/v)$ μM s^{-1}, so the appropriate conversion factor to be applied to r_h^* and V_{ATP} is 0.2×10^{15} μm^{-1}. The ATP wave is initiated by setting a step concentration (typically 10 μM) of ATP in the layer surrounding the central cell.

The equations for the diffusion of IP_3, Eq. 8, and of ATP, Eq. 11, are solved using a ''leap-frog'' method (see the Appendix in Henery (40); in the present case, only the straightforward extension of the one-dimensional case is required since there are only single equations, and not coupled equations). The other differential equations for ATP store depletion, Eq. 10, Ca^{2+}, Eq. 12, and h, Eq. 14, are solved using a standard Runge-Kutta method.

RESULTS

$P2Y_1$ and $P2Y_2$ receptor generation of Ca^{2+} in a single astrocyte

According to the model in Fig. 1 *A*, exposure of a single astrocyte to ATP leads to both an increase in $[Ca^{2+}]$ as well as the release of ATP, which increases [ATP] and then acts on P2YRs of the cell in an autocrine manner. Fig. 2 shows that exposure of an astrocyte to an initiating pulse of ATP (Fig. 2 *A*) leads to a fast increase in $[IP_3]$ (Fig. 2 *B*). Given that the release of ATP is directly coupled to IP_3 (see Eq. 9), the ATP autocrine mechanism gives rise to a relatively sustained increase in [ATP], which is terminated and drops back to basal levels as a consequence of depletion of the store of releasable ATP in the astrocyte (Fig. 2 *C*). Calcium is released from the ER by IP_3, so that there is a concomitant increase in $[Ca^{2+}]$ accompanying, but lagging that of $[IP_3]$ (Fig. 2 *D*).

The results of a sustained application of ATP to a single astrocyte are given in Fig. 3. The quantitative relation between peak $[Ca^{2+}]$ and [ATP] is shown in Fig. 3 *A*, with the curves giving higher peak Ca^{2+} as K_R decreases. Fig. 3 *B* shows that the rate of rise of $[Ca^{2+}]$, after application of a fixed concentration (5 μM) of ATP, increases with a decrease in K_R. This rate of rise also increases with an increase in [ATP] (Fig. 3 *C*). Fig. 3 *D* plots the half-rise times for $[Ca^{2+}]$ as a function of [ATP]. Shown also are the experimental values of Gallagher and Salter (15) for astrocytes in which ATP or ADP acts exclusively on $P2Y_1$ Rs (*diamonds*) or ATP acts exclusively on $P2Y_2$ Rs (*circles*). It will be noted that the theoretical curves give a best fit to the experimental data for the $P2Y_2$ Rs if $K_R \sim 5$–15 μM, but that the data for the $P2Y_1$ Rs is fitted if $K_R \sim 25$–50 μM. Thus ATP acting on $P2Y_2$ Rs gives a faster rising $[Ca^{2+}]$ than when it acts on $P2Y_1$ Rs, even though both receptors have the same sensitivity to ATP.

$P2Y_1$ and $P2Y_2$ receptor generation of Ca^{2+} and release of ATP from astrocytes

Consider a network consisting of a lane of astrocytes, each astrocyte making junctions with one another (Fig. 1 *B*), using

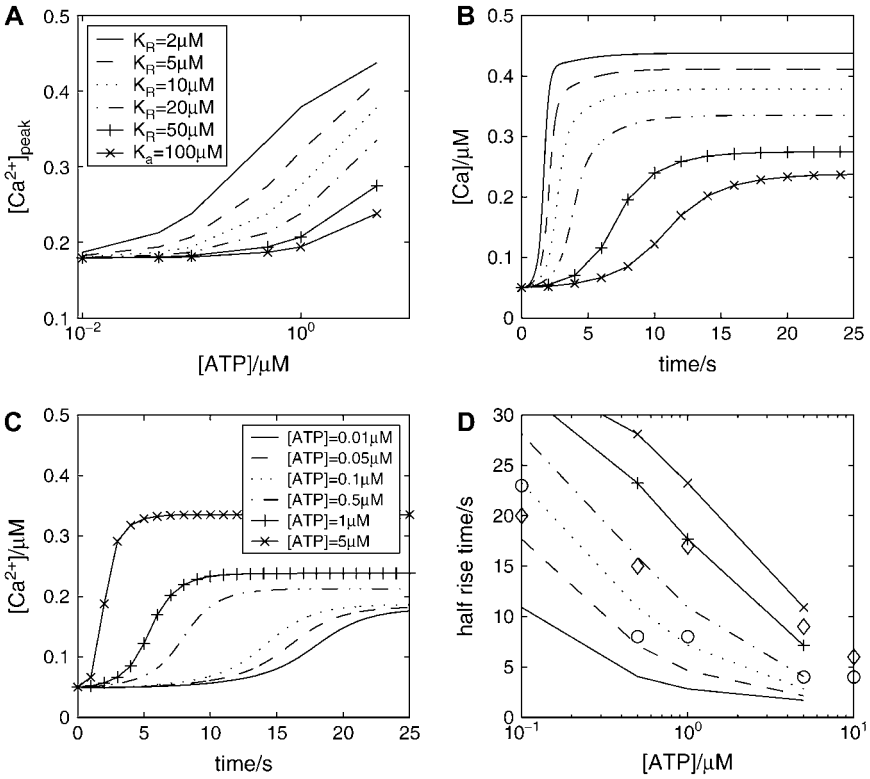

FIGURE 3 Properties of the $P2Y_1$ and $P2Y_2$ receptors on a single model astrocyte after sustained application of ATP. (*A*) Dose-response curve, with [ATP] on the abscissa (logarithmic scale) and peak Ca^{2+} on the ordinate, for receptors with K_R = 2, 5, 10, 20, 50, and 100 μM, as indicated. (*B*) Time course of Ca^{2+} in an astrocyte, after a step application of ATP (5 μM) to P2Y receptors, for the same range of K_R values as in *A*. (*C*) Time course of Ca^{2+} after the step application of various concentrations of ATP (0.01, 0.05, 0.1, 0.5, 1.0, and 5.0 μM), as indicated. $K_R = 20$ μM. (*D*) Time for Ca^{2+} to reach 50% of its peak value in response to different concentrations of ATP acting on receptors with the same range of K_R values as in *A*. Also shown is the experimental data from Fig. 6 *d* in Gallagher and Salter (15), for $P2Y_1$ receptors (*diamonds*) and $P2Y_2$ receptors (*circles*).

the transmitter ATP acting on P2YRs at the junctions. Initiation of the transmission of ATP and of Ca^{2+} waves along the network begins at a cell when the [ATP] immediately surrounding the cell is impulsively raised to 10 μM. A $[Ca^{2+}]$ transient is thus initiated in the cell, and the cell also releases ATP, which then acts back in an autocrine manner to release further ATP after this initial application. This released ATP, together with some of that applied, diffuses to the next cell to generate Ca^{2+} and also to trigger the regenerative release of ATP once more through the action of P2YRs. In this manner, the Ca^{2+} and ATP waves are transmitted along the astrocyte network.

Fig. 4 shows the quantitative relationships between [ATP] (*a*), $[IP_3]$ (*b*), the size of the ATP store in the astrocyte (*c*), and $[Ca^{2+}]$ (*d*). Some data relating to Fig. 4 is summarized in Table 2. Fig. 4, *A* and *B*, is for lanes of astrocytes one cell wide and 19 cells long with $K_R = 25$ μM in Fig. 4 *A* and $K_R = 15$ μM in Fig. 4 *B*. The changes in $[IP_3]$ in each cell are similar to those in [ATP], and they both lead the $[Ca^{2+}]$ changes. This happens because the increase in $[Ca^{2+}]$ arises only after IP_3 has acted on the calcium store through the mechanism described by Eq. 12, whereas IP_3 causes the immediate release of ATP from stores inside the cell, according to Eq. 9. The release of ATP, involving in part an autocrine mechanism, is terminated by depletion of the ATP store (Fig. 4, *Ac* and *Bc*). Comparison between the results for $K_R = 25$ μM (as for $P2Y_1$ R, Fig. 4 *A*) and $K_R = 15$ μM (as for $P2Y_2$ R, Fig. 4 *B*), shows that in the latter case the duration of $[Ca^{2+}]$ at 70% height is less, as is that of [ATP] (Table 2). This leads to a faster speed for both the ATP and

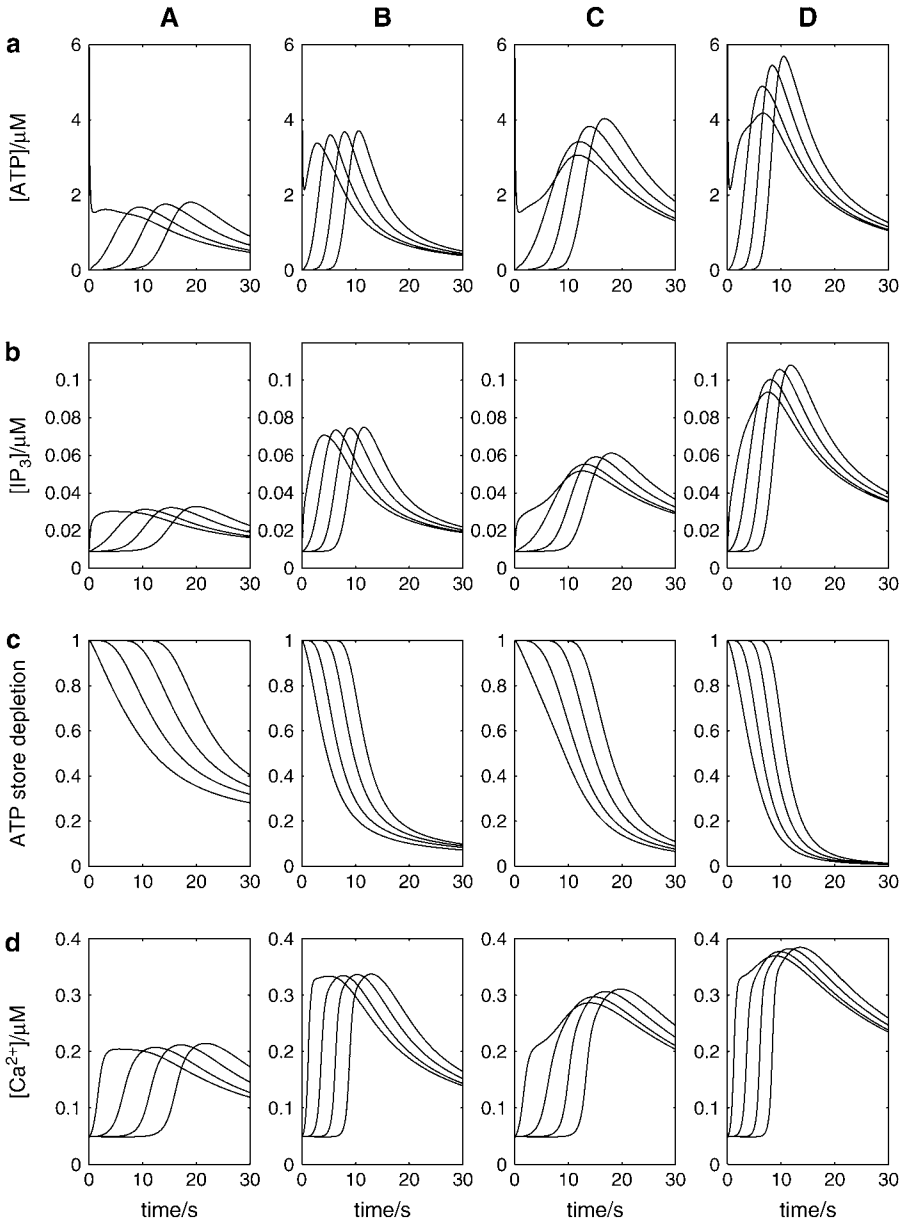

FIGURE 4 Propagation of various signals in a lane of model astrocytes. The lane is 19 cells long and either one cell wide (columns *A* and *B*) or three cells wide (columns *C* and *D*), with spacing of 50 μm between the centers of adjacent cells in all cases. Results are shown for four astrocytes (*1–4*), situated sequentially along a lane (using the *middle row* in columns *C* and *D*), with initiation occurring in the central astrocyte (number *1*). (*a*) [ATP] immediately outside each astrocyte. (*b*) IP_3 production in each astrocyte. (*c*) Depletion of the ATP store in each astrocyte. (*d*) Ca^{2+} transients in each astrocyte. $K_R = 25$ μM in columns *A* and *C* and 15 μM in columns *B* and *D*. The waves are initiated at $t = 0$ by an instantaneous pulse of ATP of magnitude 10 μM around astrocyte *1*.

TABLE 2 Data from Fig. 4; the durations are calculated at 70% of the height above background

	Lane	K_R (μM)	Wave speed (μm s^{-1})	Lag ATP-Ca^{2+} (s)	Duration (s) ATP	Duration (s) Ca^{2+}
Fig. 4 *A*	One cell wide	25	11	2.8	10	14
Fig. 4 *B*	One cell wide	15	19	2.3	4.8	11.2
Fig. 4 *C*	Three cells wide	25	16	3.0	9.4	18
Fig. 4 *D*	Three cells wide	15	23	3.0	5.9	17.6

Ca^{2+} waves (19 μm s^{-1} compared with 11 μm s^{-1} for the higher K_R). Gallagher and Salter (15) observed propagation exclusively through $P2Y_1$ R at 6 μm s^{-1} (see their Fig. 4 *e*) and through $P2Y_2$ R at 18 μm s^{-1} (see their Fig. 4 *e*). The velocities for Ca^{2+} for different values of K_R are summarized in Fig. 5 (*open bars*). For $K_R \gtrsim 33\ \mu$M the wave decreases rapidly in amplitude and does not propagate beyond the first few astrocytes from the point of stimulation. This is in marked contrast to the behavior for $K_R < 33\ \mu$M, in which case the wave propagates indefinitely with almost constant amplitude. For $K_R \gtrsim 33\ \mu$M, and an initial impulsive application of 10 μM ATP, the value of ρ (Eq. 2) is too small for the G-protein cascade to produce sufficient IP_3 to sustain the regenerative release of ATP. The decrease in duration of ATP and Ca^{2+} waves at the lower K_R is due to the faster depletion of the ATP stores by the action of IP_3 (compare Fig. 4 *Ac* with Fig. 4 *Bc*). Note also the larger amplitude of [ATP] and therefore of [Ca^{2+}] for the receptors with the smaller K_R (compare Fig. 4, *A* and *B*).

A number of calculations were also done with the inclusion of ATP breakdown, as given by the last term in Eq. 11. There was some diminution in amplitude and some decrease in velocity of the Ca^{2+} wave, but the overall results were very similar to those without this term. For example, for the parameter choice $V_{deg} = 1\ \mu$M s^{-1}, $K_{deg} = 5\ \mu$M, both the amplitude and velocity declined by $<10\%$.

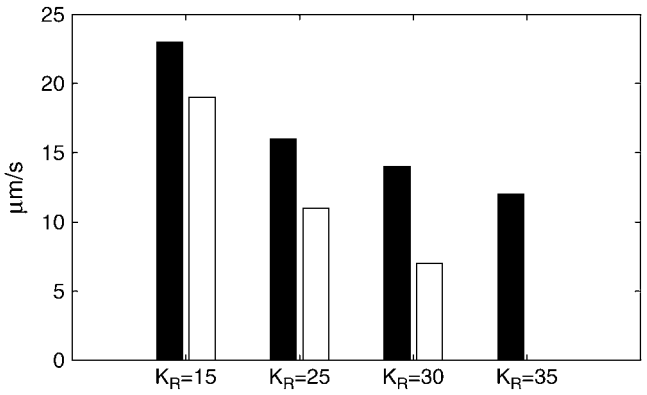

FIGURE 5 Dependence on K_R of the speed of the Ca^{2+} wave in a lane of astrocytes. The bars show the speed of the wave, from astrocyte to astrocyte, at distances $>100\ \mu$m from the point of initiation, for $K_R = 15$, 25, 30, and 35 μM. The open bars are for a lane that is one cell wide and the solid bars are for a lane that is three cells wide. For the one-cell-wide case and $K_R = 35\ \mu$M, the wave does not propagate beyond three cells, so its speed has not been calculated.

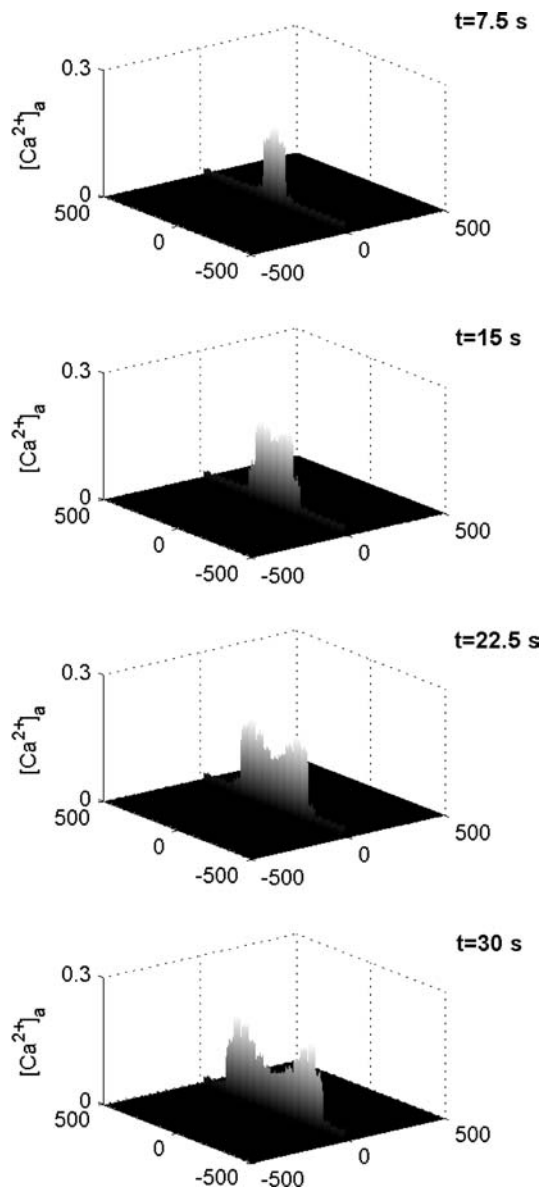

FIGURE 6 Diagrammatic representation of the spatial and temporal changes in Ca^{2+} in a network consisting of a lane of astrocytes one cell wide, the distance apart of the centers of the astrocytes being 50 μm. The calcium wave is initiated by an instantaneous pulse of ATP of concentration 10 μM at the central astrocyte at time $t = 0$. The vertical bars give Ca^{2+} in μM at times $t = 7.5$, 15, 22.5, and 30 s, as indicated. $K_R = 25\ \mu$M.

Consideration next was made of lanes of astrocytes which were three cells wide rather than just one cell. In this case, junctional transmission occurred first at the site of initiation to the immediately surrounding four astrocytes before propagating along this wider lane. Fig. 4, *C* and *D*, gives the results for cells possessing receptors with $K_R = 25\ \mu$M and 15 μM, respectively. In Fig. 4, comparison of *C* with *A* shows the effects of increasing the width of the network. For

a given K_R value, there is a substantial increase in peak [ATP] (from ~2 μM to ~4 μM) with concomitant increase in peak [Ca^{2+}] from ~0.2 μM to over 0.3 μM. Although the ATP store is depleted at a faster rate in the larger network (in Fig. 4, compare *Cc* with *Ac*), the time courses of both [ATP] and [Ca^{2+}] are not much different in the two cases (in Fig. 4, compare *Aa* and *Ad* with *Ca* and *Cd*). This occurs because the pooling of ATP in the extracellular space, by the additional astrocytes in the larger network, offsets the loss due to store depletion. The result is to increase the amplitudes of ATP and Ca^{2+} waves with some increase in their speed (Table 2; see also Fig. 5, *solid bars*).

The transmission of the Ca^{2+} wave along the length of an astrocyte network consisting of a lane of cells using receptors with $K_R = 25$ μM is shown diagrammatically in Fig. 6. At 7.5 s the Ca^{2+} transient is near its peak value at the site of initiation in the middle of the lane (compare Fig. 6 ($t = 7.5$ s) with Fig. 4 *Aa*). Thereafter the wave is transmitted with little change in peak amplitude or speed along the network from the site of initiation (Fig. 6).

The question arises as to whether changing the size of the initiating [ATP] affects the size and propagation of Ca^{2+} in the remaining astrocytes along a lane of cells. Doubling the initiating [ATP] from 10 μM (Fig. 7 *A*) to 20 μM (Fig. 7 *B*) makes little difference to either the peak amplitude of [Ca^{2+}] at the site of initiation and in the immediately adjacent cells or the speed of propagation in this vicinity or beyond the initiating region.

It has been reported that the addition of exogenous ATP can modify the propagation of Ca^{2+} in astrocytes in vivo, by increasing the distance over which the Ca^{2+} wave propagates (Sul et al. (62); see their Fig. 8). Although there is no reason why Ca^{2+} does not propagate over any distance in our model (provided K_R is not too large), it was of interest to observe if raising the ambient level of [ATP] affects the characteristics of propagation. Fig. 8 shows that the effects of increasing the ambient [ATP] from 0.03 μM to 0.07 μM are to marginally increase the speed of propagation (in Fig. 8, compare *Aa* with *Ba*) without changing the peak amplitude of the Ca^{2+} wave (in Fig. 8, compare *Ab* with *Bb*). Increasing the ambient [ATP] further, for example to 0.1 μM, leads to spontaneous production of ATP and Ca^{2+} in all cells.

$P2Y_1$ and $P2Y_2$ receptor generation of Ca^{2+} and release of ATP for a two-dimensional astrocyte network

Nearly all experimental work on astrocytes in vitro employs two-dimensional arrays of these cells (see Introduction). A study has therefore been made of transmission of ATP and Ca^{2+} waves in a two-dimensional plane of astrocytes compared with the one-dimensional lanes of astrocytes. Propagation of the Ca^{2+} wave in the two-dimensional network is

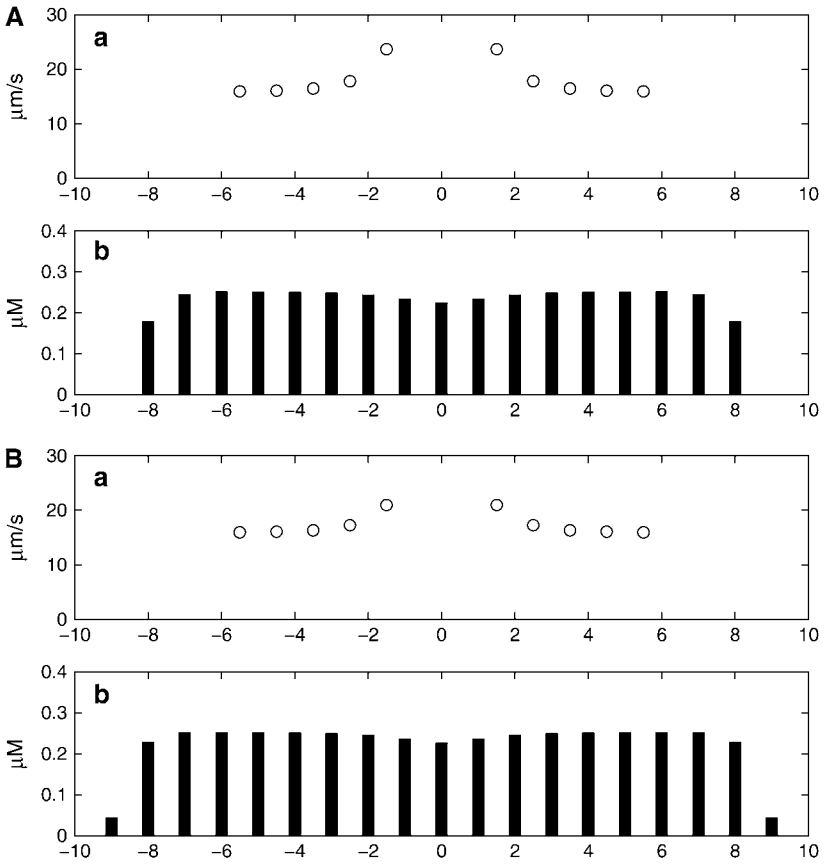

FIGURE 7 Changes in the amplitude of the Ca^{2+} wave and its speed of conduction from astrocyte to astrocyte with changes in the amplitudes of the initiating ATP transient, which is 10 μM in *A* and 20 μM in *B*. In each case, the network is a lane of astrocytes three cells wide and initiation takes place at the central astrocyte. $K_R = 25$ μM. (*a*) The speed of the Ca^{2+} wave between adjacent astrocytes. (*b*) The peak amplitude of the Ca^{2+} transient in all the astrocytes.

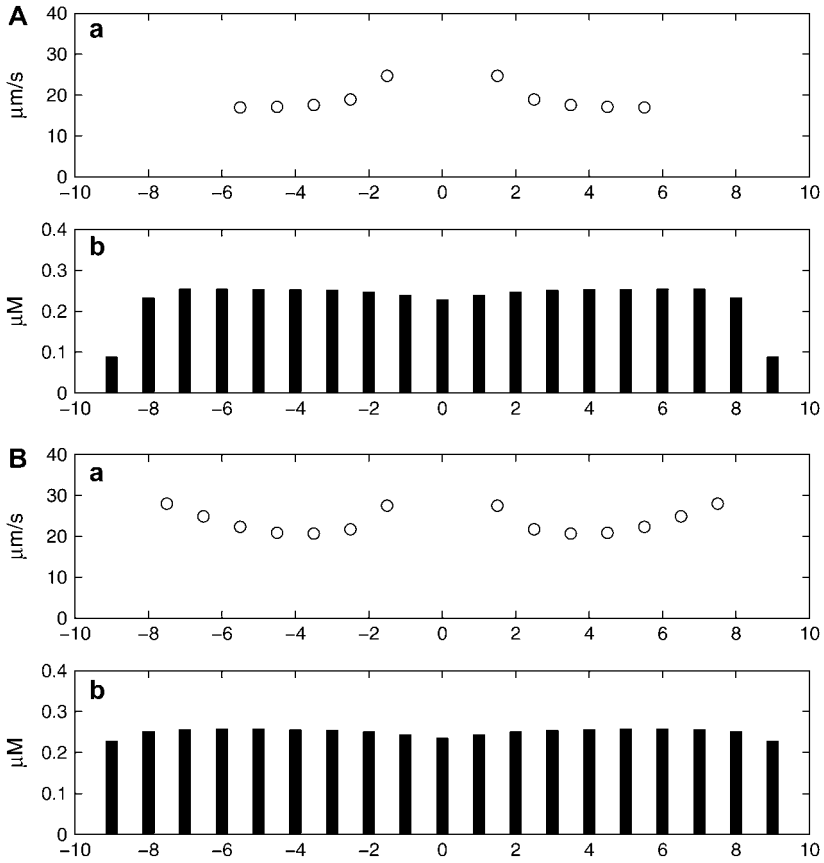

FIGURE 8 Changes in the amplitude of the Ca^{2+} wave and its speed of conduction from astrocyte to astrocyte with changes in the ambient background [ATP], which is 0.03 μM in *A* and 0.07 μM in *B*. In each case, the network is a lane of astrocytes three cells wide and initiation is a pulse of ATP of amplitude 10 μM at the central astrocyte. $K_R = 25$ μM. (*a*) The speed of the Ca^{2+} wave between adjacent astrocytes. (*b*) The peak amplitude of the Ca^{2+} transient in all the astrocytes.

illustrated diagrammatically in Fig. 9 *A*. This shows the wave-front moving out in the plane from its site of initiation in the center. There is an increase in the rates of rise and peak amplitude of [ATP] and [Ca^{2+}] between the one-dimensional case (a lane one cell wide, Fig. 4 *A*) and the two-dimensional case in which each cell has four nearest neighbors with centers 50 μm apart (Fig. 9 *B*). The rate of decline of the ATP store is greater in the two-dimensional case (compare Fig. 4 *Ac* with Fig. 9 *Bc*), but the rate of decline of [ATP], [IP_3], and hence [Ca^{2+}], is slower in the two-dimensional case because of the higher pooling of ATP (compare Fig. 4 *A* with Fig. 9 *B*). The duration of [Ca^{2+}] at half-peak is >30 s (after the wave-front has moved away from the site of initiation; see Fig. 9 *Bd*), which is similar to that observed by Wang et al. (14) (see their Fig. 4 *C*). The [ATP] wave has a shorter duration than the Ca^{2+} wave (Fig. 9, *Ba* and *Bd*), as is also observed ((14), their Fig. 4 *B*).

Experiments have been performed on Ca^{2+} propagation in which two-dimensional cultures of astrocytes are manipulated in such a way as to produce an astrocyte-free lane surrounded by astrocytes (see, for example, Fig. 1 *B* in Hassinger et al. (13)). Propagation of the Ca^{2+} wave is at ~10 μm s^{-1} in the absence of the lane (see Fig. 2 *A* in Hassinger et al. (13)). Successively wider lanes delay the propagation across the lane by successively longer times, consistent with the time taken for diffusion of ATP across the lane to initiate a Ca^{2+} wave in astrocytes on the opposite side of the lane from the side of the mechanically initiated Ca^{2+} wave. An 80-μm lane gave a delay of 18 s (see Fig. 2 *B* in Hassinger et al. (13)). Our model of Ca^{2+} transmission reproduces many of these features of Ca^{2+} propagation across cell-free lanes. Fig. 10 shows the effects of initiating Ca^{2+} transmission in lanes of cells that are either one cell wide (Fig. 10 *A*) or three cells wide (Fig. 10 *B*), when there are parallel lanes of cells on each side of the central lane containing the initiating cell, but the lanes are separated by a 75-μm-wide gap. At $t = 22.5$ s (for $K_R = 25$ μM), there is clear indication that the Ca^{2+} has jumped to the adjacent lanes in both cases.

The present model gave a delay of 12 s for a 75-μm lane and 22 s for a 125-μm-wide lane (see Fig. 11 *B*), with a propagation speed of 16 μm s^{-1} in the absence of lanes (Fig. 11 *A*), if $K_R = 25$ μM. In the case where $K_R = 15$ μM, the model gave a delay of 8 s for a 75-μm-wide lane (Fig. 11 *B*) with a propagation speed of 25 μm s^{-1} in the absence of lanes (Fig. 11 *A*). For $K_R = 25$ μM, a jump of 175 μM can occur after ~40 s (Fig. 11 *B*).

DISCUSSION

ATP versus gap-junction transmission

There are considerable contradictions in the literature concerning the question of whether transmission between astrocytes

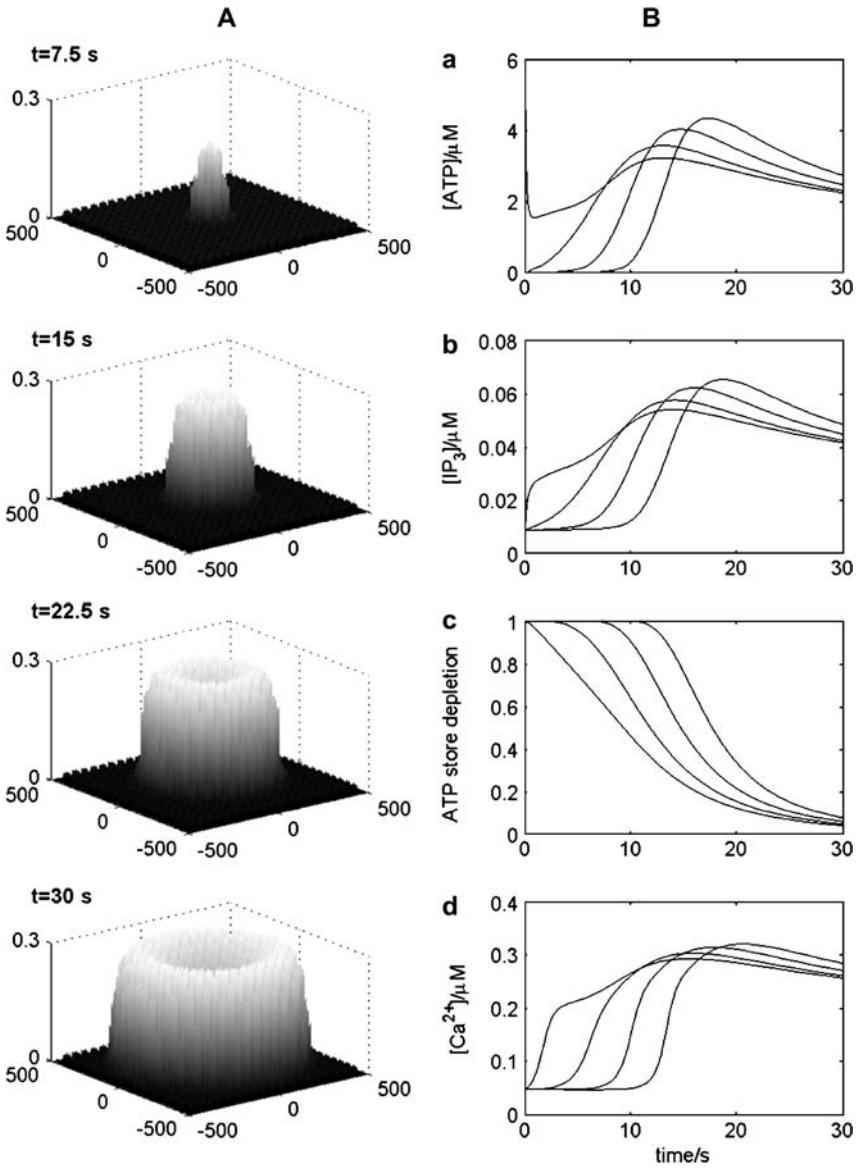

FIGURE 9 Diagrammatic representation of the spatial and temporal changes in a network consisting of a regular array of cells in a plane, the distance apart of the centers of the astrocytes being 50 μm. The calcium wave is initiated by an instantaneous pulse of ATP of concentration 10 μM around the central astrocyte at time $t = 0$. (*A*) The Ca^{2+} response in the whole array, with the vertical bars giving Ca^{2+} in μM at times $t = 7.5$, 15, 22.5, and 30 s, as indicated. (*B*) Results for four model astrocytes (*1–4*), at sequentially greater distances along a line in the array, with initiation occurring in astrocyte *1*. $K_R = 25$ μM. (*a*) [ATP] immediately outside each astrocyte. (*b*) IP_3 production in each astrocyte. (*c*) Depletion of the ATP store in each astrocyte. (*d*) Ca^{2+} transients in each astrocyte.

is chemical, involving the release of ATP, or involves gap junctions (for some reviews of the earlier literature, see Charles (41) and Giaume and Venance (42)). For example, blocking gap junctions between astrocytes in the striatum with 18-α-glycyrrhetinic acid is reported to block Ca^{2+} propagation (43–46); blocking these junctions with heptanol blocks 85% of propagation between spinal cord astrocytes (47) and 75% of propagation between cortical astrocytes (48,49). On the other hand, it has been shown that Ca^{2+} propagation is considerably antagonized by purinergic receptor blockade between cortical astrocytes (50) and completely antagonized by such blockade of spinal cord astrocytes (17,15). Some of these apparent contradictions may be attributed to the gap-junction blockers acting to antagonize ATP release (51) and/or to the linkage between purinergic receptor (P2YR) expression and that of connexins (47). Whether endogenous endonucleotidases of astrocytes play a role in limiting access of ATP to $P2Y_1$ Rs and $P2Y_2$ Rs is controversial, as some say that it does (52) and others that it does not (15). We have not included any gap-junction transmission mechanism in our model of astrocyte junctions, although this might be necessary in the future when better agreement is reached on the relative contributions of gap junctions and ATP to the Ca^{2+} transmission process.

ATP release mechanisms

As pointed out in the Introduction, the mechanism by which ATP is released by astrocytes has not yet been elucidated as there are contradictory observations on this point. ATP

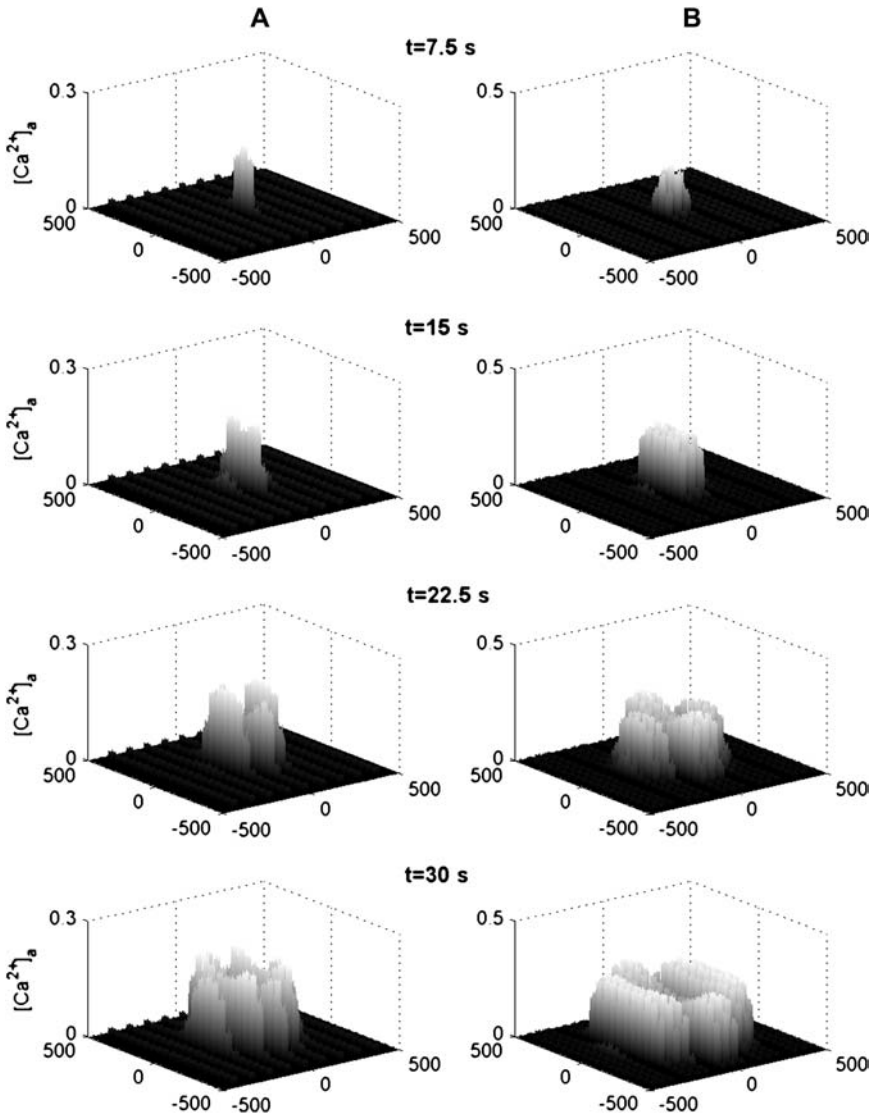

FIGURE 10 Diagrammatic representation of the spatial and temporal changes in Ca^{2+} in a network consisting of (*A*) parallel lanes of astrocytes one cell wide separated by empty lanes one cell wide and (*B*) parallel lanes of astrocytes three cells wide separated by empty lanes one cell wide. The remaining details are as for Fig. 6.

release, due to mechanical or chemical stimulation, has been reported as either unaffected by the blocking of Ca^{2+} with thapsigargin or BAPTA/AM chelators (14,53), or affected by such blocking (26,25). A calcium-independent release of ATP may occur via anion transporters (28,9). Connexin hemichannels that are permselective for ATP release (54) have also been implicated in ATP release from astrocytes (55), as well as from endothelial cells (56), so that a product of G-protein signaling could be envisaged as opening such channels. However, it has been claimed that connexin blockers, such as oleamide, fail to block transmission between astrocytes (57), whereas the connexin hemichannel activator quinine evokes ATP release (58). These uncertainties point to a lack of specificity of these agents and suggest that a knockout of specific connexin genes is needed to establish the role of these in astrocyte transmission (59). We have therefore opted at this stage for a Ca^{2+}-independent release of ATP from astrocytes in our model. This is supported by the observation that the ATP wave appears to precede the Ca^{2+} wave in a number of experimental situations (27,14).

Modeling transmission of the Ca^{2+} wave

Transmission at junctions between astrocytes has previously been modeled only in terms of gap junctions mediating transmission (30). It is assumed in these models that there is direct diffusion of inositol trisphosphate (IP_3) between apposing astrocytes at the junctions, with IP_3 generated by a Ca^{2+}-sensitive PLC process in addition to the PLC generation of IP_3 after G-protein receptor activation. Given the considerable recent evidence that the major component of junctional transmission involves the release of ATP, at least for astrocytes originating from certain parts of the central nervous system, we have developed a model of this process of transmission.

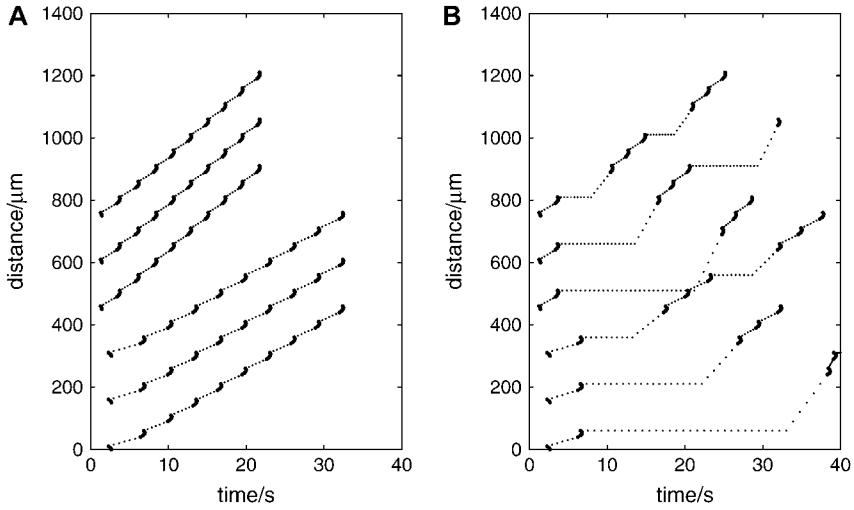

FIGURE 11 Transmission of the Ca^{2+} wave along lanes and across cell-free lanes. The network consists of parallel lanes three cells wide separated by cell-free lanes of various widths. The Ca^{2+} wave is initiated at $t = 0$ by a pulse of ATP of amplitude 10 μM applied to the central astrocyte. (*A*) The time at which $[Ca^{2+}]$ reaches half-maximum in each astrocyte situated along the center of the middle lane. The points (·) show the time at which Ca^{2+} is half-maximum at each grid point inside an astrocyte, the grid points being taken along the central line. The dotted line interpolates between these points and has no physical significance. The upper set of three traces is for $K_R = 15$ μM and the lower set is for $K_R = 25$ μM. In each set, starting from the top, the width of the cell-free lanes has been increased by one cell width; thus it is respectively 75, 125, and 175 μm. The speed in the absence of cell-free lanes is 23 μm s^{-1} for $K_R = 15$ μM and 16 μm s^{-1} for $K_R = 25$ μM. For clarity, each subsequent trace has been displaced by 150 μm, so the ordinate gives relative distance. (Compare with Fig. 2 *A* in Hassinger et al. (13).) (*B*) As for *A*, except the times at which $[Ca^{2+}]$ reaches half-maximum are now plotted for a lines of grid points passing through the centers of astrocytes lying transverse to the lanes and thus the Ca^{2+} wave has to cross cell-free lanes. Again, the dotted lines link corresponding data but have no physical significance. The delays for propagation of Ca^{2+} across the cell-free lanes of widths 75, 125, and 175 μM are, for $K_R = 15$ μM (from the top down), 7, 13, and 21 s, respectively; and for $K_R = 25$ μM, they are 10, 19, and 30 s, respectively.

Modeling conduction of the Ca^{2+} wave

Single astrocytes, when exposed to a ligand such as noradrenaline, release calcium from different endoplasmic reticula in such a way that the process can be modeled as a series of Ca^{2+}-coupled oscillators, each of these being equivalent to one ER (60). An individual ER or oscillator is activated by IP_3 generated throughout at the astrocyte plasmalemma by the action of the ligand on G-protein coupled receptors found over the surface of the plasmalemmal membrane. In the present model, IP_3 is also generated throughout the plasmalemma membrane of the astrocyte, but in this case the generation is due to the action of ATP and not noradrenaline. However, this IP_3 then diffuses through the astrocyte to act on ER found at each of the 125 grid points in the numerical representation of the astrocyte and to release Ca^{2+} at each of them. We have not apportioned specialized ER at the grid points, possessing relative high densities of IP_3 receptors, which participate in a calcium-coupled oscillator system as is the case in the model of Roth et al. (60). The incorporation of such specialized ER does not assist in illuminating the ATP transmission mechanisms that are the point of interest or the present work.

Spatial and temporal characteristics of Ca^{2+} wave propagation and transmission in astrocyte networks

In the presence of neurons, astrocytes propagate a Ca^{2+} wave from a point of mechanical stimulation for a distance of 150−250 μm (61,62) and from a point of potassium stimulation for ~1000 μm (63), there being indications of a diminution in amplitude and speed over the first 150 μm (for a review see Giaume and Venance (42)). In the absence of neurons, Ca^{2+} waves propagate for at least 200 μm from a point of stimulation (see, for example, Takano et al. (64)). However, it is not known if the Ca^{2+} wave propagates in an all-or-none fashion over long distances (>200 μm) when only glial cells are present, although it has been argued that propagation is limited to an approximate distance of 60 astrocytes (42). There is no restriction on the distance of propagation of the Ca^{2+} wave in the present model, which is regenerative due to the mechanism of ATP-induced ATP release. However, increasing the dissociation constant (K_R) of receptors slows the velocity of propagation of the Ca^{2+} wave from its site of initiation, and if K_R is increased to 35 μM in a single lane of astrocytes, propagation ceases at 100 μm from the site of initiation (see Fig. 5). As pointed out in Receptors, above, K_R is an effective dissociation constant and may take values greater than the actual dissociation constant for ATP acting on P2Y receptors. Ectonucleotidases may act to metabolize released ATP (65). As described in Results, above, introduction of such enzymes into our model merely uniformly decreases the amplitude and velocity of the Ca^{2+} wave from its point of origin, without affecting the propagation distance. It remains to be seen whether Ca^{2+} is observed to propagate for distances of >1000 μm in continuous astrocyte networks confined to discrete lanes in the absence of neurons, such as those modeled in Fig. 6 *A*.

The speed of propagation of the Ca^{2+} wave is critically dependent on the dissociation constant, K_R, of the receptors (see Table 2 and Fig. 5). Gallagher and Salter (15) obtained velocities of 8 μm s^{-1} and 16 μm s^{-1} for propagation of the

Ca^{2+} wave through the release of ATP at astrocyte junctions using $P2Y_1$ and $P2Y_2$ receptors, respectively. This range of velocities is approximately that observed in cultured astrocytes from a variety of sources (see Table 1 in Giaume and Venance (42)). According to the present model, there is a slight decrease in the speed of propagation of the Ca^{2+} wave over the first three or so astrocytes from the site of initiation ($\sim$150 μm), but there is no diminution in the peak amplitude of Ca^{2+} (see Figs. 7 and 8). It has been suggested that the relatively high velocities and amplitudes of Ca^{2+} waves in the vicinity of mechanical stimulation arise as a consequence of a combination of gap junction communication and chemical transmission at the astrocyte junctions at the site of mechanical stimulation (41,64). We have not yet included gap junctions in our model to test this idea; however, it seems implausible that adding a slow process (gap junction communication) to a faster process (extracellular transmission) will result in an overall increase in speed. A further point concerns the common experimental procedure in which Ca^{2+} release is initiated by mechanical stimulation of an astrocyte. If this only increases $[IP_3]$ in the stimulated cell, as has been suggested (66,14), then our method of initiation using a sudden increase in [ATP] surrounding the cell would be equivalent (see Eq. 9). It is interesting in this regard that doubling the step increase in extracellular ATP makes very little difference to the speed or peak amplitudes of the Ca^{2+} wave (see Fig. 7).

Critical tests of the purinergic junction model of astrocyte transmission

As mentioned in the Introduction, Hassinger et al. (13) examined in some detail the extent to which Ca^{2+} waves could jump cell free gaps of different widths. They found that there was a delay in propagation of the Ca^{2+} wave across lanes which increased with gap width until this reached $\sim$150 μm, when such propagation failed. For a 80-μm-wide cell-free lane the delay was 18 s, whereas our model of this process gave for a 125-μm-wide cell-free lane a delay of 14 s for astrocytes with $K_R = 15$ μM. More recent research has used micropatterned arrays of astrocytes in which lanes of cells $\sim$110-μm-wide alternate with cell-free lanes $\sim$40-μm-wide, with mechanical initiation of Ca^{2+} occurring in just one lane (64). These authors obtained a delay of $\sim$10 s for the Ca^{2+} wave to traverse the cell-free lane. This may be compared with a delay of 8 s, which our model gives for a cell-free lane of width 75 μm for astrocytes with a $K_R = 30$ μM. The velocities in the experimental studies were 8–20 μm s^{-1}, which are those found in the modeling study for P2Y receptors with K_R values of $\sim 35-25$ μM, respectively. These quantitative comparisons between experimental and modeling results suggest that the model can account for these observations on micropatterned arrays of astrocytes.

We thank Dr. Greg Lemon for his input in formulating the present model.

This work was supported by Australian Research Council grant No. DP0345968.

REFERENCES

1. Nobile, M., I. Monaldi, S. Alloisio, C. Cugnoli, and S. Ferroni. 2003. ATP-induced, sustained calcium signalling in cultured rat cortical astrocytes: evidence for a non-capacitative, P2X7-like-mediated calcium entry. *FEBS Lett.* 538:71–76.
2. Neary, J. T., R. Laskey, C. van Breemen, J. Blicharska, L. O. Norenberg, and M. D. Norenberg. 1991. ATP-evoked calcium signal stimulates protein phosphorylation/dephosphorylation in astrocytes. *Brain Res.* 566:89–94.
3. Shiga, H., T. Tojima, and E. Ito. 2001. Ca^{2+} signaling regulated by an ATP-dependent autocrine mechanism in astrocytes. *Neuroreport.* 12:2619–2622.
4. Koizumi, S., Y. Saito, K. Nakazawa, K. Nakajima, J. I. Sawada, S. Kohsaka, P. Illes, and K. Inoue. 2002. Spatial and temporal aspects of Ca^{2+} signaling mediated by P2Y receptors in cultured rat hippocampal astrocytes. *Life Sci.* 72:431–442.
5. Ballerini, P., M. P. Rathbone, P. Di Iorio, A. Renzetti, P. Giuliani, I. D'Alimonte, O. Trubiani, F. Caciagli, and R. Ciccarelli. 1996. Rat astroglial P2Z (P2X7) receptors regulate intracellular calcium and purine release. *Neuroreport.* 7:2533–2537.
6. Idestrup, C. P., and M. W. Salter. 1998. P2Y and P2U receptors differentially release intracellular Ca^{2+} via the phospholipase C/inositol 1,4,5-triphosphate pathway in astrocytes from the dorsal spinal cord. *Neuroscience.* 86:913–923.
7. Bruner, G., and S. Murphy. 1993. Purinergic P2Y receptors on astrocytes are directly coupled to phospholipase A2. *Glia.* 7:219–224.
8. Centemeri, C., C. Bolego, M. P. Abbracchio, F. Cattabeni, L. Puglisi, G. Burnstock, and S. Nicosia. 1997. Characterization of the Ca^{2+} responses evoked by ATP and other nucleotides in mammalian brain astrocytes. *Br. J. Pharmacol.* 121:1700–1706.
9. Abdipranoto, A., G. J. Liu, E. L. Werry, and M. R. Bennett. 2003. Mechanisms of secretion of ATP from cortical astrocytes triggered by uridine triphosphate. *Neuroreport.* 14:2177–2181.
10. King, B. F., J. T. Neary, Q. Zhu, S. Wang, M. D. Norenberg, and G. Burnstock. 1996. P2 purinoceptors in rat cortical astrocytes: expression, calcium-imaging and signalling studies. *Neuroscience.* 74:1187–1196.
11. Zhu, Y., and H. K. Kimelberg. 2001. Developmental expression of metabotropic $P2Y_1$ and $P2Y_2$ receptors in freshly isolated astrocytes from rat hippocampus. *J. Neurochem.* 77:530–541.
12. Fumagalli, M., R. Brambilla, N. D'Ambrosi, C. Volonte, M. Matteoli, C. Verderio, and M. P. Abbracchio. 2003. Nucleotide-mediated calcium signaling in rat cortical astrocytes: role of P2X and P2Y receptors. *Glia.* 43:218–303.
13. Hassinger, T. D., P. B. Guthrie, P. B. Atkinson, M. V. Bennett, and S. B. Kater. 1996. An extracellular signaling component in propagation of astrocytic calcium waves. *Proc. Natl. Acad. Sci. USA.* 93:13268–13273.
14. Wang, Z., P. G. Haydon, and E. S. Yeung. 2000. Direct observation of calcium-independent intercellular ATP signaling in astrocytes. *Anal. Chem.* 72:2001–2007.
15. Gallagher, C. J., and M. W. Salter. 2003. Differential properties of astrocyte calcium waves mediated by $P2Y_1$ and $P2Y_2$ receptors. *J. Neurosci.* 23:6728–6739.
16. Salter, M. W., and J. L. Hicks. 1994. ATP-evoked increases in intracellular calcium in neurons and glia from the dorsal spinal cord. *J. Neurosci.* 14:1563–1575.
17. Fam, S. R., C. J. Gallagher, and M. W. Salter. 2000. $P2Y_1$ purinoceptor-mediated Ca^{2+} signaling and Ca^{2+} wave propagation in dorsal spinal cord astrocytes. *J. Neurosci.* 20:2800–2808.

18. Fam, S. R., C. J. Gallagher, L. V. Kalia, and M. W. Salter. 2003. Differential frequency dependence of $P2Y_1$- and $P2Y_2$-mediated Ca^{2+} signaling in astrocytes. *J. Neurosci.* 23:4437–4444.

19. Ralevic, V., and G. Burnstock. 1998. Receptors for purines and pyrimidines. *Pharmacol. Rev.* 50:413–492.

20. Bernardinelli, Y., P. J. Magistretti, and J. Y. Chatton. 2004. Astrocytes generate Na^+-mediated metabolic waves. *Proc. Natl. Acad. Sci. USA.* 101:14937–14942.

21. Pasti, L., M. Zonta, T. Pozzan, S. Vicini, and G. Carmignoto. 2001. Cytosolic calcium oscillations in astrocytes may regulate exocytotic release of glutamate. *J. Neurosci.* 21:477–484.

22. Bezzi, P., V. Gundersen, J. L. Galbete, G. Seifert, C. Steinhauser, E. Pilati, and A. Volterra. 2004. Astrocytes contain a vesicular compartment that is competent for regulated exocytosis of glutamate. *Nat. Neurosci.* 7:613–620.

23. Zhang, Q., M. Fukuda, E. Van Bockstaele, O. Pascual, and P. G. Haydon. 2004. Synaptotagmin IV regulates glial glutamate release. *Proc. Natl. Acad. Sci. USA.* 101:9441–9446.

24. Zhang, Q., T. Pangrsic, M. Kreft, M. Krzan, N. Li, J. Y. Sul, M. Halassa, E. Van Bockstaele, R. Zorec, and P. G. Haydon. 2004. Fusion-related release of glutamate from astrocytes. *J. Biol. Chem.* 279:12724–12733.

25. Cotrina, M. L., J. H. Lin, A. Alves-Rodrigues, S. Liu, J. Li, H. Azmi-Ghadimi, J. Kang, C. C. Naus, and M. Nedergaard. 1998. Connexins regulate calcium signaling by controlling ATP release. *Proc. Natl. Acad. Sci. USA.* 95:15735–15740.

26. Coco, S., F. Calegari, E. Pravettoni, D. Pozzi, E. Taverna, P. Rosa, M. Matteoli, and C. Verderio. 2003. Storage and release of ATP from astrocytes in culture. *J. Biol. Chem.* 278:1354–1362.

27. Newman, E. A. 2001. Propagation of intercellular calcium waves in retinal astrocytes and Müller cells. *J. Neurosci.* 21:2215–2223.

28. Ballerini, P., P. Di Iorio, R. Ciccarelli, E. Nargi, I. D'Alimonte, U. Traversa, M. P. Rathbone, and F. Caciagli. 2002. Glial cells express multiple ATP binding cassette proteins which are involved in ATP release. *Neuroreport.* 13:1789–1792.

29. Sneyd, J., M. Wilkins, A. Strahonja, and M. J. Sanderson. 1998. Calcium waves and oscillations driven by an intercellular gradient of inositol (1,4,5)-trisphosphate. *Biophys. Chem.* 72:101–109.

30. Höfer, T., L. Venance, and C. Giaume. 2002. Control and plasticity of intercellular calcium waves in astrocytes: a modeling approach. *J. Neurosci.* 22:4850–4859.

31. Lemon, G., W. G. Gibson, and M. R. Bennett. 2003. Metabotropic receptor activation, desensitization and sequestration-I: modelling calcium and inositol 1,4,5-trisphosphate dynamics following receptor activation. *J. Theor. Biol.* 223:93–111.

32. Wu, D., and N. Mori. 1999. Extracellular ATP-induced inward current in isolated epithelial cells of the endolymphatic sac. *Biochim. Biophys. Acta.* 1419:33–42.

33. Charles, A. C., J. E. Merrill, E. R. Dirksen, and M. J. Sanderson. 1991. Intercellular signaling in glial cells: calcium waves and oscillations in response to mechanical stimulation and glutamate. *Neuron.* 6:983–992.

34. Kim, W. T., M. G. Rioult, and A. H. Cornell-Bell. 1994. Glutamate-induced calcium signaling in astrocytes. *Glia.* 11:173–184.

35. Keizer, J., and L. Levine. 1996. Ryanodine receptor adaptation and Ca^{2+}-induced Ca^{2+} release-dependent Ca^{2+} oscillations. *Biophys. J.* 71:3477–3487.

36. Fink, C. F., B. Slepchenko, and L. M. Loew. 1999. Determination of time-dependent inositol-1,4,5-trisphosphate concentrations during calcium release in a smooth muscle cell. *Biophys. J.* 77:617–628.

37. De Young, G. W., and J. Keizer. 1992. A single-pool inositol 1,4,5-trisphosphate-receptor-based model for agonist-stimulated oscillations in Ca^{2+} concentration. *Proc. Natl. Acad. Sci. USA.* 89:9895–9899.

38. Li, Y.-X., and J. Rinzel. 1994. Equations for $InsP_3$ receptor-mediated (Ca^{2+}) oscillations derived from a detailed kinetic model: a Hodgkin-Huxley like formalism. *J. Theor. Biol.* 166:461–473.

39. Bushong, E. A., M. E. Martone, Y. Z. Jones, and M. H. Ellisman. 2002. Protoplasmic astrocytes in CA1 stratum radiatum occupy separate anatomical domains. *J. Neurosci.* 22:183–192.

40. Henery, R., W. G. Gibson, and M. R. Bennett. 1997. Quantal currents and potential in the three-dimensional anisotropic bidomain model of smooth muscle. *Bull. Math. Biol.* 59:1047–1075.

41. Charles, A. 1998. Intercellular calcium waves in glia. *Glia.* 24:39–49.

42. Giaume, C., and L. Venance. 1998. Intercellular calcium signaling and gap junctional communication in astrocytes. *Glia.* 24:50–64.

43. Venance, L., J. Cordier, M. Monge, B. Zalc, J. Glowinski, and C. Giaume. 1995. Homotypic and heterotypic coupling mediated by gap junctions during glial cell differentiation in vitro. *Eur. J. Neurosci.* 7:451–461.

44. Venance, L., D. Piomelli, J. Glowinski, and C. Giaume. 1995. Inhibition by anandamide of gap junctions and intercellular calcium signalling in striatal astrocytes. *Nature.* 376:590–594.

45. Venance, L., N. Stella, J. Glowinski, and C. Giaume. 1997. Mechanism involved in initiation and propagation of receptor-induced intercellular calcium signalling in cultured rat astrocytes. *J. Neurosci.* 17:1981–1992.

46. Venance, L., J. Premont, J. Glowinski, and C. Giaume. 1998. Gap junctional communication and pharmacological heterogeneity in astrocytes cultured from the rat striatum. *J. Physiol.* 510:429–440.

47. Scemes, E., S. O. Suadicani, and D. C. Spray. 2000. Intercellular communication in spinal cord astrocytes: fine-tuning between gap junctions and P2 nucleotide receptors in calcium wave propagation. *J. Neurosci.* 20:1435–1445.

48. Frisch, C., M. Theis, M. A. De Souza Silva, E. Dere, G. Sohl, B. Teubner, K. Namestkova, K. Willecke, and J. P. Huston. 2003. Mice with astrocyte-directed inactivation of connexin43 exhibit increased exploratory behaviour, impaired motor capacities, and changes in brain acetylcholine levels. *Eur. J. Neurosci.* 18:2313–2318.

49. Suadicani, S. O., M. H. De Pina-Benabou, M. Urban-Maldonado, D. C. Spray, and E. Scemes. 2003. Acute downregulation of Cx43 alters P2Y receptor expression levels in mouse spinal cord astrocytes. *Glia.* 42:160–171.

50. Cotrina, M. L., J. H. Lin, and M. Nedergaard. 1998. Cytoskeletal assembly and ATP release regulate astrocytic calcium signaling. *J. Neurosci.* 18:8794–8804.

51. Bennett, M. R., L. Farnell, W. G. Gibson, Y. Q. Lin, and D. H. Blair. 2001. Quantal and non-quantal current and potential fields around individual sympathetic varicosities on release of ATP. *Biophys. J.* 80:1311–1328.

52. Joseph, S. M., M. R. Buchakjian, and G. R. Dubyak. 2003. Colocalization of ATP release sites and ecto-ATPase activity at the extracellular surface of human astrocytes. *J. Biol. Chem.* 278:23331–23342.

53. Anderson, C. M., J. P. Bergher, and R. A. Swanson. 2004. ATP-induced ATP release from astrocytes. *J. Neurochem.* 88:246–256.

54. Goldberg, G. S., A. P. Moreno, and P. D. Lampe. 2002. Gap junctions between cells expressing connexin 43 or 32 show inverse permselectivity to adenosine and ATP. *J. Biol. Chem.* 277:36725–36730.

55. Cotrina, M. L., J. H. Lin, J. C. López-Garcia, C. C. Naus, and M. Nedergaard. 2000. ATP-mediated glia signalling. *J. Neurosci.* 20: 2835–2844.

56. Gomes, P., S. R. Srinivas, W. Van Dressche, J. Vereecke, and B. Himpens. 2005. ATP release through connexin hemichannels in corneal endothelial cells. *Invest. Ophthalmol. Vis. Sci.* 46:1208–1218.

57. Guan, X., B. F. Cravatt, G. R. Ehring, J. E. Hall, D. L. Boger, R. A. Lerner, and N. B. Gilula. 1997. The sleep-inducing lipid oleamide deconvolutes gap junction communication and calcium wave transmission in glial cells. *J. Cell Biol.* 139:1785–1792.

58. Stout, C. E., J. L. Costantin, C. C. Naus, and A. C. Charles. 2002. Intercellular calcium signaling in astrocytes via ATP release through connexin hemichannels. *J. Biol. Chem.* 277:10482–10488.

59. Theis, M., D. Speidel, and K. Willecke. 2004. Astrocyte cultures from conditional connexin43-deficient mice. *Glia*. 46:130–141.

60. Roth, B. J., S. V. Yagodin, L. Holtzclaw, and J. T. Russell. 1995. A mathematical model of agonist-induced propagation of calcium waves in astrocytes. *Cell Calcium*. 17:53–64.

61. Muyderman, H., M. Nilsson, F. Blomstrand, S. Khatibi, T. Olsson, E. Hansson, and L. Ronnback. 1998. Modulation of mechanically induced calcium waves in hippocampal astroglial cells. Inhibitory effects of α1-adrenergic stimulation. *Brain Res*. 793:127–135.

62. Sul, J.-Y., G. Oorosz, R. S. Givens, and P. G. Haydon. 2004. Astrocyte connectivity in the hippocampus. *Neuron Glia Biol*. 1:3–11.

63. Peters, O., C. G. Schipke, Y. Hashimoto, and H. Kettenmann. 2003. Different mechanisms promote astrocyte Ca^{2+} waves and spreading depression in the mouse neocortex. *J. Neurosci*. 23:9888–9896.

64. Takano, H., J. Y. Sul, M. L. Mazzanti, R. T. Doyle, P. G. Haydon, and M. D. Porter. 2002. Micropatterned substrates: approach to probing intercellular communication pathways. *Anal. Chem*. 74:4640–4646.

65. Zimmermann, H., N. Braun, B. Kegel, and P. Heine. 1998. New insights into molecular structure and function of ectonucleotidases in the nervous system. *Neurochem. Int*. 32:421–425.

66. Niggel, J., W. Sigurdson, and F. Sachs. 2000. Mechanically induced calcium movements in astrocytes, bovine aortic endothelial cells and C6 glioma cells. *Membr. Biol*. 174:121–134.

67. Bennett, M. R., L. Farnell, W. G. Gibson, and S. Karunanithi. 1995. Quantal transmission at purinergic junctions: stochastic interaction between ATP and its receptors. *Biophys. J*. 68:925–935.